RESEARCH ARTICLE

A novel laser-assisted approach for synthesis of AuNPs/PS nanostructures as photodetector

Anita S. Alber[1] · Falah A-H. Mutlak[1]

Abstract This paper propose to construct a photodetector with ultra-high sensitivity using a laser ablation process. Formed AuNPs by Nd: YAG laser wavelength of 1064 nm and 532 nm, 500 pulses and different energies on porous silicon etched for 18 min. Morphology, structural, optical and *J–V* characteristic for AuNPs/PS has been investigated. By changing the parameters of the laser such as wavelength and energy and comparing between them, the SEM particle size decrease with increasing of wavelength and the XRD become more broad in 1064 nm than in 532 nm. The high-energy side of the PL spectrum's peak shifts a little, showing that quantum confinement is having an impact in AuNPs/PS. Photo-detector properties of AuNPs show the first exhibits responsivity when it absorbs an Au nanoparticle in the visible 600 nm wavelength region. The PS layer's ability to absorb visible light at 850 nm is shown by its responsivity in the second area maximum quantum efficiency in 532 nm is 94% and increased in 1064 nm to 95.6%. Based on this high-quality photodiode, the AuNPs/PS generated by laser ablation build great photodetectors that may be a feasible option for industrial photoelectric purposes.

✉ Anita S. Alber
anitaalber989@gmail.com

1 Department of Physics, College of Science, University of Baghdad, Baghdad, Iraq

Introduction

Gold nanoparticles (AuNPs) can be created by alternative techniques, such as physical irradiation process, laser ablation, electrochemical, chemical methods, and biological method, microorganisms, plants [1–3]. As a result nanoparticles/porous Si (NP/PS) systems made of metal have been investigated in enhancing their sensing capabilities [4, 5] and luminescent [6–8] PS substrates surface enhanced Raman scattering covered in noble metal nanoparticles, such as Gold and Silver, have also been widely researched [9–14]. Hydrodynamic disturbances on polished Si substrates, also the thin-film thickness fluctuations, voids occur in the film, with little effect from the substrate topography [15–21]. Surface Plasmon Resonance (SPR) is one of the most important optical properties of metallic nanoparticles. It is formed of collective oscillations of conduction electrons caused by the electromagnetic field of incident light [22]. Nanoparticles have several properties which aren't found in bulk materials [23]. The shape and size of nanoparticles have a profound effect on their properties (electrical, optical, and magnetic) [24]. AuNPs are interesting nanomaterial with a large range of applications in basic research. [25, 26] AuNPs, for example, have been employed in single electron devices and scanning laser microscopy studies of cellular mechanisms [27, 28]. Ultrasensitive biosensors, catalysis in the manufacture of self-assembling nanomaterial, photovoltaic devices, and nonlinear optics [29–34]. Nanoscale materials can be used in a range of applications, such as optomechanical sensors, chemicals, and natural cycles [35–37]. Laser ablation in liquids has recently been mentioned as a possible source of nanoparticles by a few authors [38–41]. Gold nanoparticles (AuNPs) are particularly essential in metal nanoparticles due to their great effectiveness of (SPR) [42–45]. AuNPs have electrical, mechanical, and physical properties due to

their wide range of applications [46–48]. The absorption of AuNPs is influenced by their diameter, the electrical insulator's center, and the chemical environment [49, 50]. In AuNPs, the conduction band and valence bar are closely enough, permitting electrons to pass freely across them. These free electrons absorb the Surface Plasmon Resonance (SPR), which also is formed by the amplitude fluctuating of the electrons of nanoparticles in resonance with the optical wave [51, 52]. A new approach to produce nanoparticles that can be employed in a variety of applications is to use laser ablation in liquid. PLAL has been used to generate a variety of nanoparticles, including metals, oxides, alloys, and semiconductors [53–59]. In the current work, AuNPs that were prepared using laser ablation technology approach and deposited on PS to create ultra-high sensitivity photo detector nanostructures. Investigations have been done into the electric, optical, and structural characteristics.

Experimental details

AuNPs have been made using laser ablation (Nd:YAG) 1 Hz pulse repetition rate with wavelengths of 1064 nm and 532 nm, energies (600, 800, 1000)mJ. High pure gold plate was washed by ethanol and distilled water then placed in vessel with solution of PVA and distilled water after mixing it to the point of homogeneity using the stirrer. Production of gold nanoparticles in PVA by nanosecond laser incidence on gold plate. To obtain an appropriate concentration of gold nanoparticle solution, this experiment has been carried out multiple times, via casting technique the Au/PVA in different energies solution dripping on the porous silicon carefully prepared using photoelectrochemical etching (PECE) in 18 min. The (J–V) in dark and (J_{ph}–V) in light properties

of the structural elements Si, PS and AuNPs/PS were investigated, taking into account the light and dark current density. These samples were illuminated with a halogen lamp at a range of light power density of (5, 20, 60, and 125) mW/cm^2 with reverse voltages between (-6 and $+6$) Volt.

Results and discussion

UV–Vis absorption-based solutions using PVA were investigated for their effectiveness in both 532 nm and 1064 nm with (600, 800, 1000) mJ and 500 pulse Fig. 1 their results are compared. The intensification of the increase in laser energy can also lead to an increase in absorption spectra attributed to the rise in nanoparticles concentration. Absorbance is calculated using Beer-Lambert equation and the concentration of the solution. The formation of some more than one gap in nanoparticles, on the other hand, can result in a particle size increase. In this work, PVA 1064 nm was

Table 1 The UV–Vis characteristics for Au NPs in PVA prepared by laser ablation 532 nm and 1064 nm laser wavelength

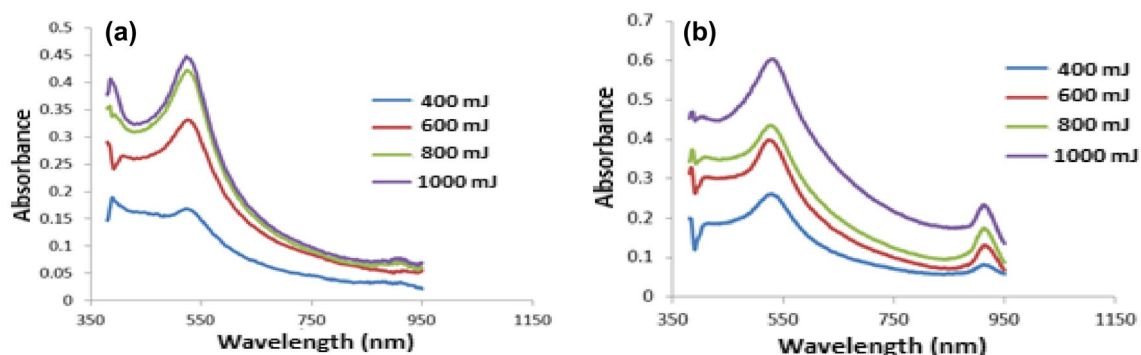| Sample	Energy (mJ)	λ max (nm)	Abs	FWMH
	400	522.5	0.080589	63.1
Au NPs-532 nm	600	513.2	0.335331	109.6
	800	516.7	0.36068	119.3
	1000	512.5	0.971448	143
	400	508.1	0.248426	98
	600	508.7	0.398437	124
Au NPs-1064 nm	800	511.8	0.417838	146
	1000	520.3	0.595543	157

Fig. 1 Absorption spectra of AuNPs colloidal prepared with various laser energies, at 500 shots. **a** 532 nm, **b** 1064 nm laser wavelength

selected for better results, as from Table 1 and compared with the rest of the table it was seen, the spectrum shows strong absorption between (500 and 550) nm and shifts toward shorter wavelengths (blue shift) with an increasing laser energy due to reduce the nanoparticles size.

XRD was used to investigate the crystalline degree of AuNPs/PS at 1064 nm and 532 nm in 1000 mJ. The XRD measurements for PS show a very strong peak in $2\theta = 69°$, $60°$ in 532 nm and $2\theta = 69°$, $70°$ in 1064 nm for 1000 mJ observed through Fig. 2. There are peaks in the XRD pattern for the AuNPs/PS layers, from the creation of crystalline AuNPs on the PS substrate, and the results for the AuNPs/PS layers we can see the layers exhibited a peak at $2\theta = 37.900°$ to the PS (111) layer in 532 nm $2\theta = 38.200°$ in 1064 nm matching to the (111) crystal planes of crystalline AuNPs, demonstrating the discovery of AuNPs when deposited on PS.

Table 2 displays the discovered crystallite sizes in Au/NPs/PS in 532 nm in 1000 mJ and PS etched in 18 min

calculated by Scherrer equation show a considerable increase in crystallite size with decreasing in FWHM in all wavelengths.

Different laser energies (600 mJ, 800 mJ, and 1000 mJ) were used to examine the PL spectra of porous silicon and AuNPs at room temperature, at two wavelengths 532 nm and 1064 nm as Fig. 3. There is only one unique emission band at (581, 588, 591) nm in 532 nm, and 1064 nm (581, 582, 588) nm. As laser pulse energy increases from 400 mJ, 600 mJ, to 1000 mJ. When comparing of two crystals, the crystal with the shorter wavelength 532 nm has a larger refractive index with longer wavelengths and lower energies, and we note in it the greatest wavelength in the visible region at 591 nm and peaks shifted to higher wavelength.
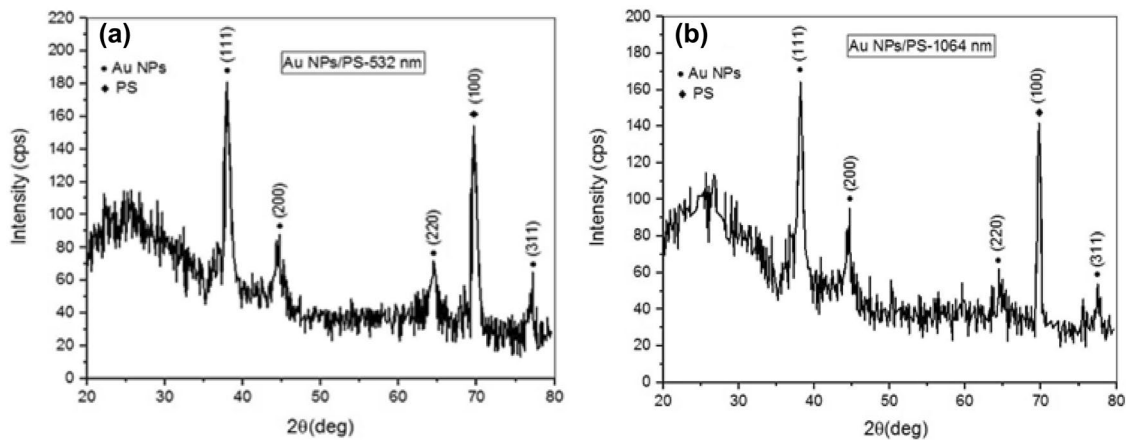
$$E = \frac{hc}{\lambda} \qquad (1)$$

Fig. 2 X-ray diffraction patterns of the Au NPs/PS prepared by laser ablation with **a** 532 nm laser wavelength, **b** 1064 nm laser wavelength

Table 2 Values obtained from measurements using XRD peaks for Au NPs/PS in PVA prepared by laser ablation with 532 nm and 1064 nm laser wavelength

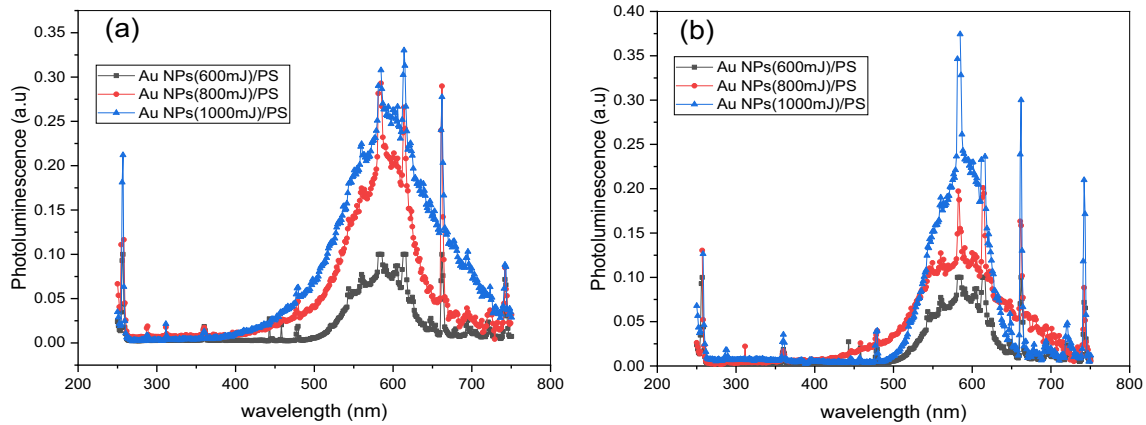| Sample	Miller indices	2 theta (°)	FWHM (°)	d_{hkl} (Å)	Crystallite size (nm)
	(111)	37.9	1.79	2.37	4.7
	(200)	44.7	1.72	2.02	5.0
Au NPs/PS-532 nm	(220)	64.5	1.60	1.44	5.9
	(311)	77.2	1.50	1.23	6.8
	(111)	38.2	2.40	2.35	3.5
	(200)	44.7	2.10	2.02	4.1
Au NPs/PS-1064 nm	(220)	64.4	1.90	1.44	4.9
	(311)	77.5	1.60	1.23	6.4

Fig. 3 PL spectra of the Au/NPs porous silicon, different laser pulse energies, Nd: YAG laser at **a** 532 nm, **b** 1064 nm laser wavelength

Table 3 Values of PL peaks AuNPs/PS prepared with varying laser pulse energies at (a) 532 nm laser wavelength (b) 1064 nm laser wavelength

Sample	Energy (mJ)	Λ (nm)	E_g (ev)	n
	600	581.2	2.133	1.853
Au NPs/PS-532 nm	800	588.2	2.108	1.862
	1000	591.2	2.097	1.863
	600	581.1	2.133	1.859
	800	582.3	2.129	1.859
Au NPs/PS-1064 nm	1000	585.3	2.118	1.861

$$n = \sqrt{1 + \frac{A}{B + E_g}} \qquad (2)$$

$A = 13.6$ eV and $B = 3.4$ eV; h, Plank constant; c, speed of light.

Using Eq. (1) [60], as the energy rate rises, the band gap (E_g) narrows, and the wavelength increases as a result the quantum confinement phenomenon when the refractive index raises Eq. (2) [61, 62]. Excitation value for PL spectra of 591 nm in 532 nm and 585 nm in 1064 nm is visible, showing a change to blue in the band gap when contrasted to bulk Si, for which the quantum confinement effect is responsible as shown in Table 3.

The particle size of AuNPs is seen in TEM images in Fig. 4. The AuNPs were created using a laser with pulse energy of 1000 mJ, 500 pulse rate in two crystal wavelength 532 nm and 1064 nm. It can be seen that prepared AuNPs nearly has a spherical shape. Complementary contrast was visible in TEM images, confirming the creation
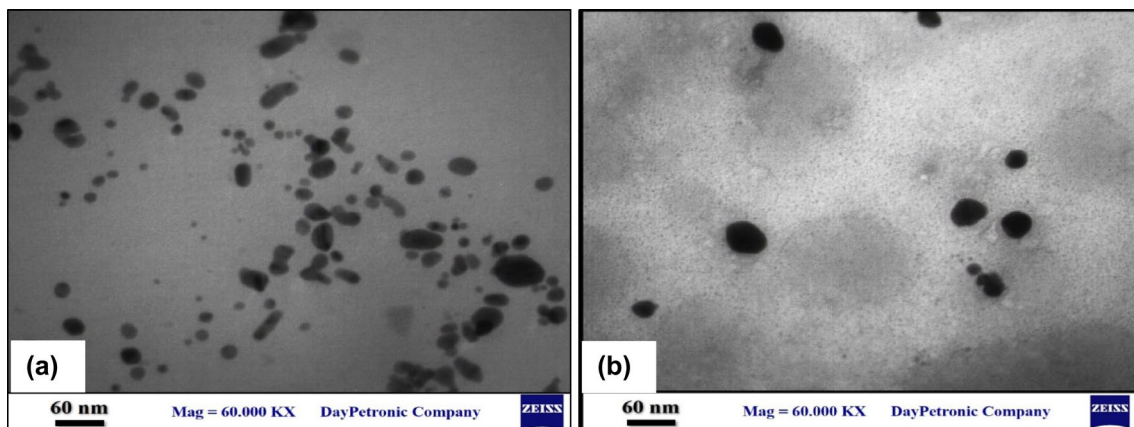

Fig. 4 TEM image for AuNPs colloidal prepared using PLAL synthesis at $E = 1000$ mJ **a** 532 nm, **b** 1064 nm laser wavelength
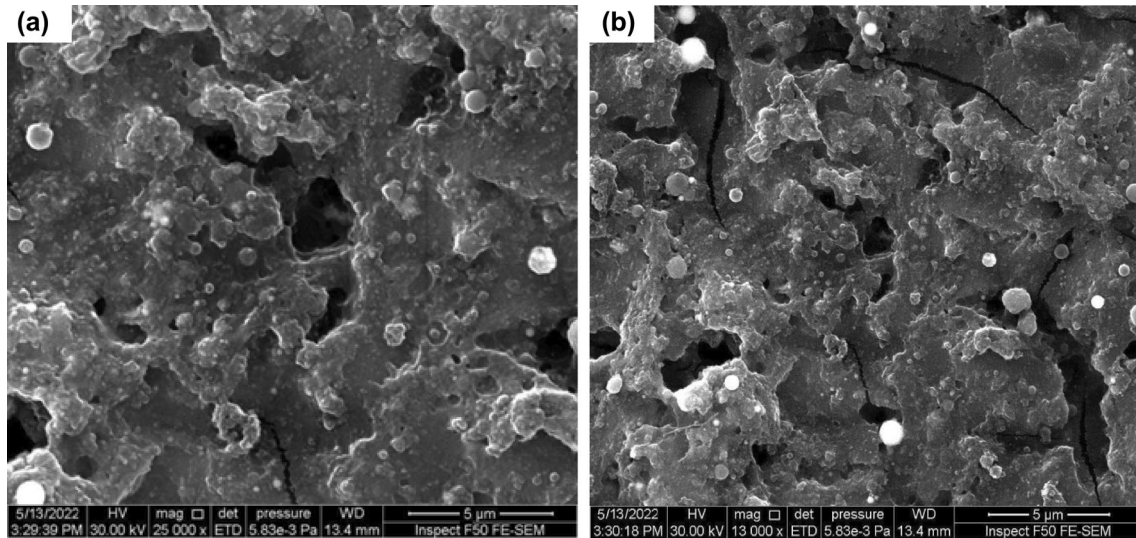
Fig. 5 SEM image of AuNPs/PS synthesized by laser ablation **a** 532 nm, **b** 1064 nm laser wavelength
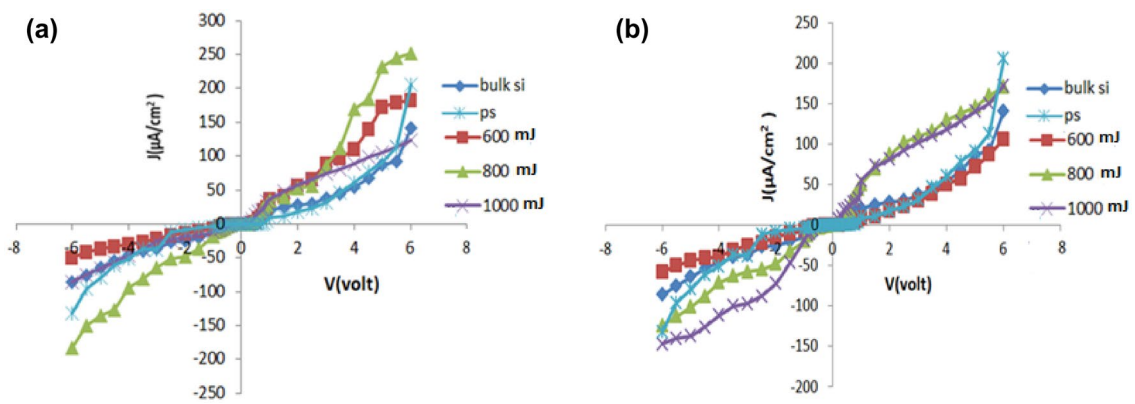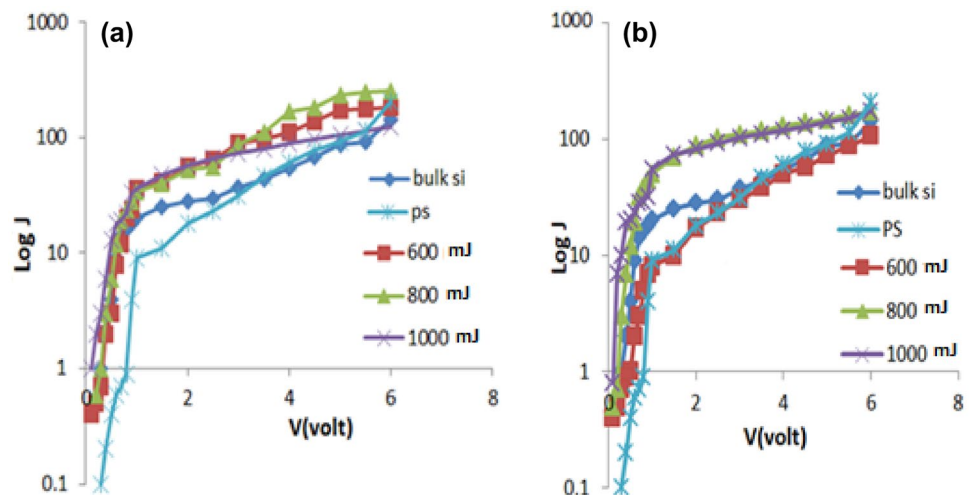

Fig. 6 *J–V* characteristic under the dark of bulk Si, PS and AuNPs/PS with various laser pulse energies **a** 532 nm, **b** 1064 nm laser wavelength

Fig. 7 log(*J*) with bias voltage of c-Si, PS and AuNPs Porous silicon at various laser energies, 500 pulses and laser wavelength (**a**) 532 nm, (**b**) 1064 nm on PS substrate under dark

of the core shell structures, it can be suggested that the uniform layer covers the spherical core the second phase. When comparing the two crystals, it becomes clear that at the wavelength of 532 nm the size of the particles is greater than 1064 nm.

Table 4 Value of saturation current, ideality factor, and barrier height of c-Si, PS and AuNPs/PS samples at various laser energies, etching time 18 min with varied laser wavelength

Sample	Wavelength (nm)	n	J_s (µA/cm^2)	Φ_{Bn} (eV)
Bulk Si		1.932	25	0.659
PS		1.326	18	0.667
AuNPs (600 mJ)/PS	532	2.288	23	0.601
AuNPs (800 mJ)/PS		1.262	70	0.632
AuNPs (1000 mJ)/PS		1.374	73	0.631
AuNPs (600 mJ)/PS	1064	1.173	37	0.679
AuNPs (800 mJ)/PS		0.8448	34	0.651
AuNPs (1000 mJ)/PS		1.809	36	0.649

The SEM images of the AuNPs Porous silicon structure in two crystals of different wavelengths and constant energy were used at 1000 mJ and the etching time of the porous silicon was fixed in 18 min the particle size increase with the crystal of 532 nm and decrease with 1064 nm so it is an inverse relationship Fig. 5.

The *J–V* characteristics of AuNPs/PS/n-Si occur in Fig. 6 in dark circumstances with a current density of 20 mA/cm^2, an etched time of 18 min, and an HF of 16%. At laser energies of 600, 800, and 1000 mJ, it appears the current rises with the presence of AuNPs on the PS layer. Because of high electrical conductivity of the AuNPs, current increases with compared to the PS sample and decreases in contrast to bulk Si due to the high degree of crystallized form.

The streaming recombination current is not uniformly spread through the structure, as seen Fig. 7 by the comparison log (*J*) with bias voltage of AuNPs porous silicon usually at local area. The ideal factor and barrier height Φ_{Bn} calculated according to Eqs. (3) and (4) because electrons do not have enough energy to cross the barrier height, there is a lot of recombination between excited electrons and holes. The most recent is known as diffusion current, which occurs at higher voltages and results in an exponential rise in output current [63].
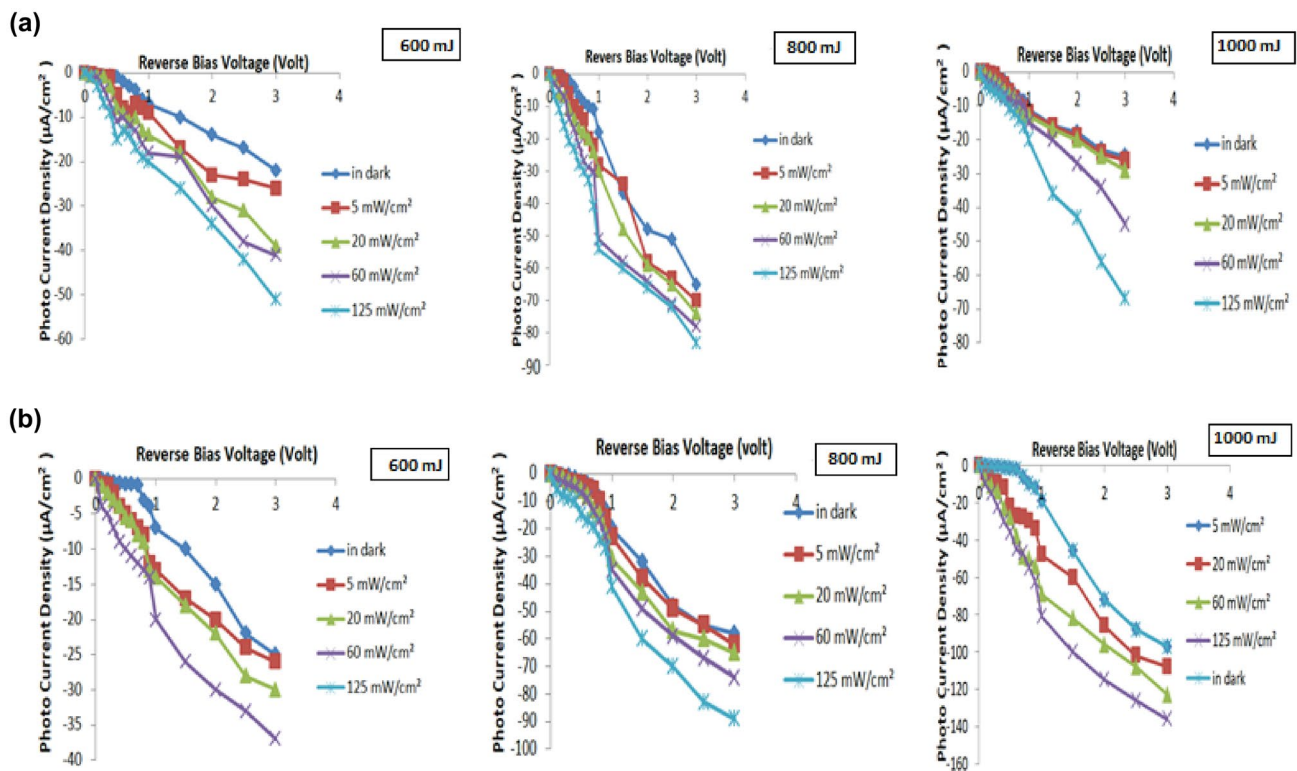

Fig. 8 J_{ph}–V curve of AuNPs/PS n-type substrate when light with varied laser wavelength (**a**) 532 nm, (**b**) 1064 nm

$$\Phi_{Bn} = \frac{K_B T}{q} \ln \left(\frac{A^{**} T^2}{J} \right) \tag{3}$$

$$n = \frac{q}{K_B T} \frac{dv}{d(\ln J)} \tag{4}$$

J, forward current density (μA/cm^2), k_B, Boltzmann constant (1.38×10^{-23} J/K), V, the applied voltage, A^{**}, represents the value of Richardson's constant (112 A/cm^2 K).

Ideality factor (n) calculated heterojunctions have barrier heights (Bn) between (0.60 and 0.62) eV in 532 nm and increasing from 0.64 to 0.679 eV in 1064 nm. These values range from 1. 2 to 2.2 for 532 nm and from 1.1 to 1.8 for 1064 nm. Applied low applied voltage to the saturation current density is obtained from the linear region of the semilog forward I–V curves (Js) (Table 4).

Figure 8 demonstrates the sandwich structure with a reverse bias voltage and some light. When PS is coated with Au film using various wavelengths of laser deposition, photocurrent increases (532 and 1064 nm). By shining light on the junctions additionally, the reverse bias current was improved, which is anticipated of the formation of electron–hole pairs in the zone of energy depletion of the incoming photons exceeds the sandwich structure's smallest immediate band gap. Conclusions of the previous studies clearly reveal that these sandwich arrangements possess a good light response, making it a better material for optoelectronic device fabrication.

Figure 9 shows the spectra of AuNPs divided two distinct portions the first shows responsiveness as a result of the near infrared ~ 600 nm wavelength region of Au nanoparticle absorption. Responsivity, the second section, shows how the PS layer absorbs visible light 850 nm. These findings enhanced the compatibility of Au with PS structures, enhancing the performance of porous silicon. The responsivity is calculated by using Eq. (5)
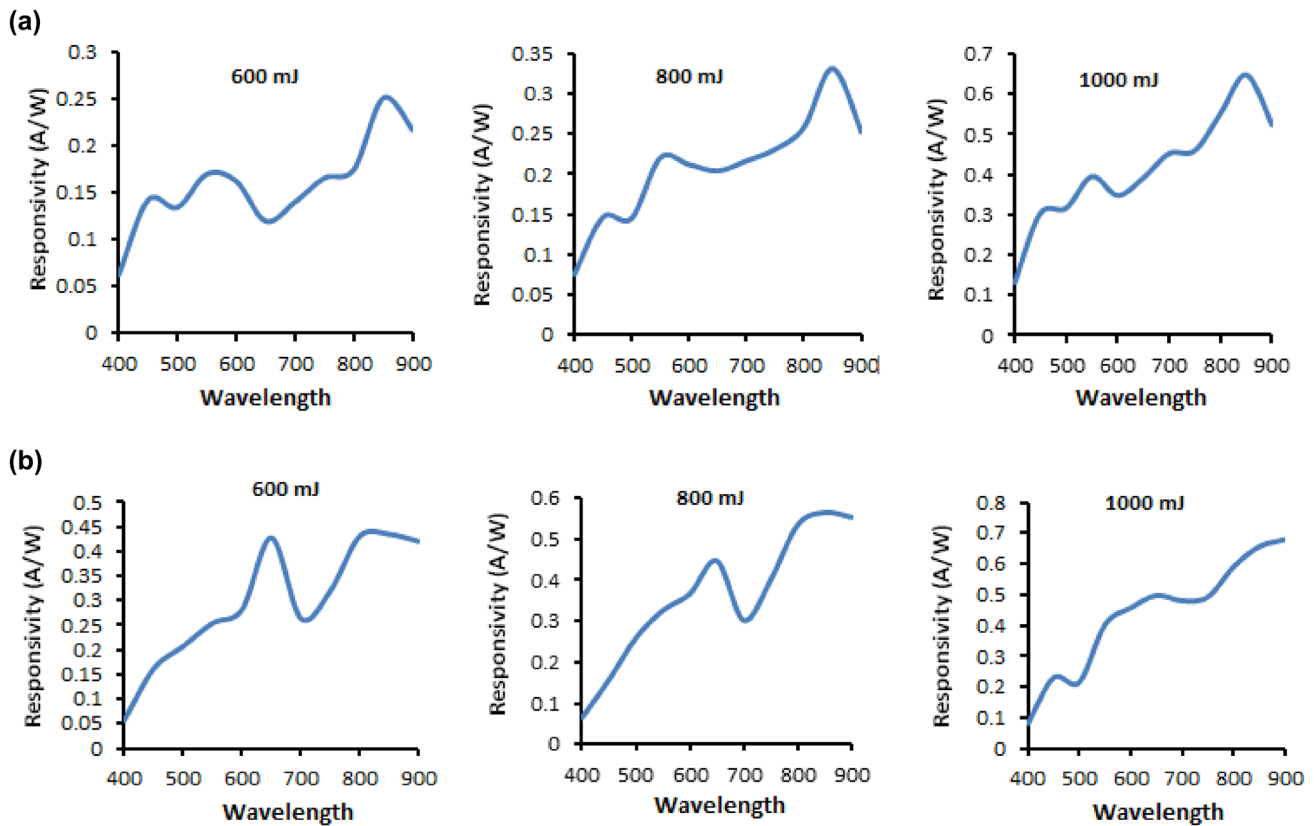
$$R_\lambda = \frac{I_{ph}}{P_{in}} \tag{5}$$

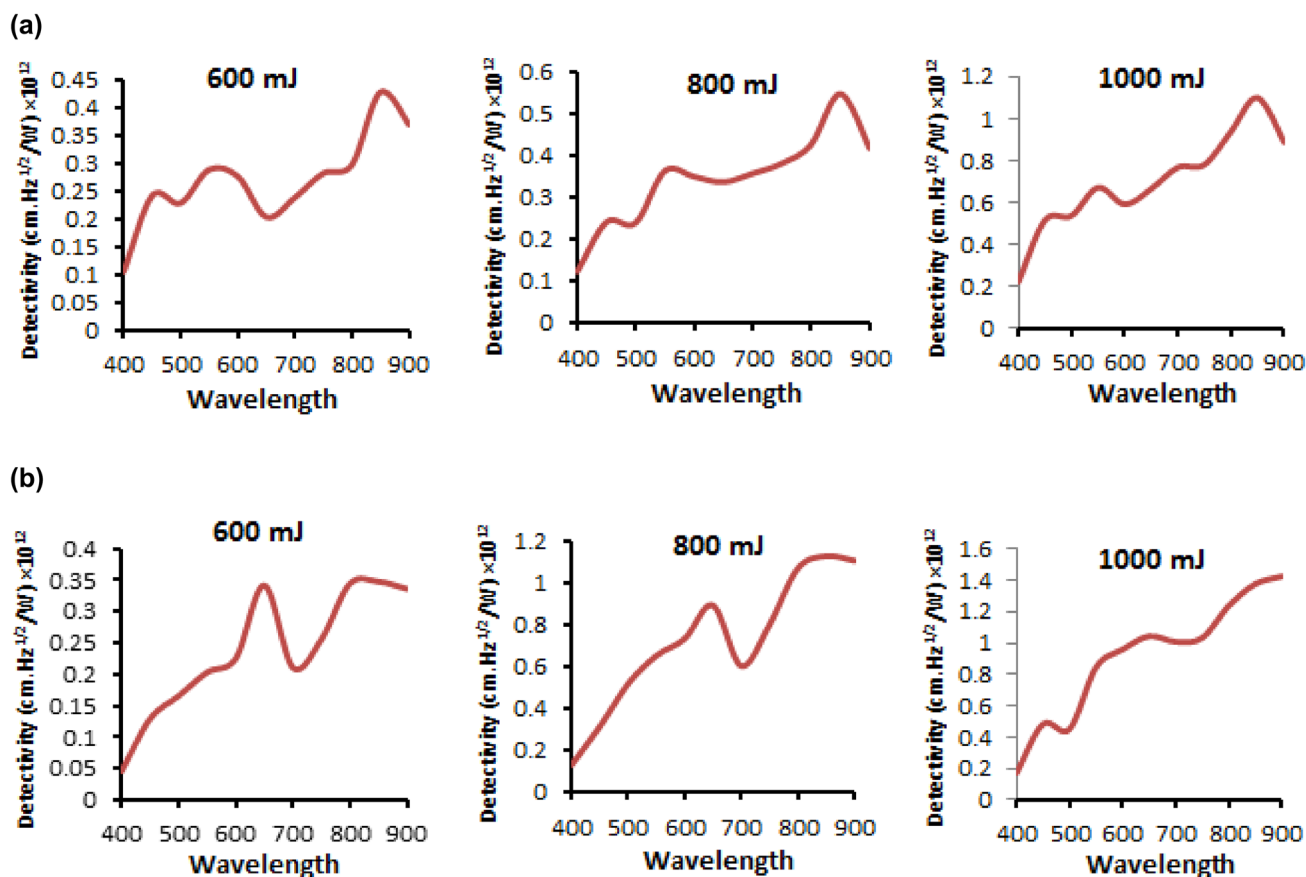**Fig. 9** Responsivity of AuNPs produced on PS substrate with varied laser wavelength (**a**) 532 nm, (**b**) 1064 nm

(a)

(b)

Fig. 10 Detectivity of AuNPs produced on PS substrate with varied laser wavelength (**a**) 532 nm, (**b**) 1064 nm

I_{ph}, current of the optical container, P_{in}, input power, Spectral responsivity R_λ is the detector signal.

Figure 10 demonstrates measurement of detectivity D^* at various wavelengths nm, to altered wavelength laser deposition 532 nm, and 1064 nm. The highest values are around (0.39260385, 0.497405712, and 0.945842868) (cm Hz$^{1/2}$/W)$\times 10^{12}$, which increase with increasing energies 600, 800, 1000 mJ in wavelength 532 nm, and (0.815409152, 0.85192001, and 0.973185088) in wavelength 1064, which match to visible energies of (532, 1064) nm, including both. Calculated detectability by Eq. (6) [64, 65].

$$D^* = \frac{\sqrt{S_{det}\Delta f}}{NEP} \tag{6}$$

The detector active area (S_{det}), which represents the noise equivalent power, and detectivity (D^*), which reflects the response of the frequency.

The link between the quantum effectiveness of the device and the wavelength of the incident light is depicted in Fig. 11. Quantum efficiency increased as the band gap of the structure widened. It was high at the time because quantum efficiency is proportional to R. Maximum quantum efficiency is determined to be 29.9% in 600 mJ, 49.7% in 800 mJ, and 94.5 in 1000 mJ at wavelength 800 nm and (66.7%, 85.1%, 95.6%) in 1064 nm crystal (600, 800, 1000 mJ). The spectral responsiveness and the quantum efficiency are determined by Eq. (7) [66–68].

$$\eta = \frac{h\upsilon}{q}R_\lambda \tag{7}$$

As the bandgap of the structure grew larger, the quantum efficiency improved. The highest efficiency was 95.6%when separate lasers, 532 nm and 1064 nm, were used to deposition thin layer. The efficiency increased with energy gap dropped, laser deposition wavelengths expanded. The
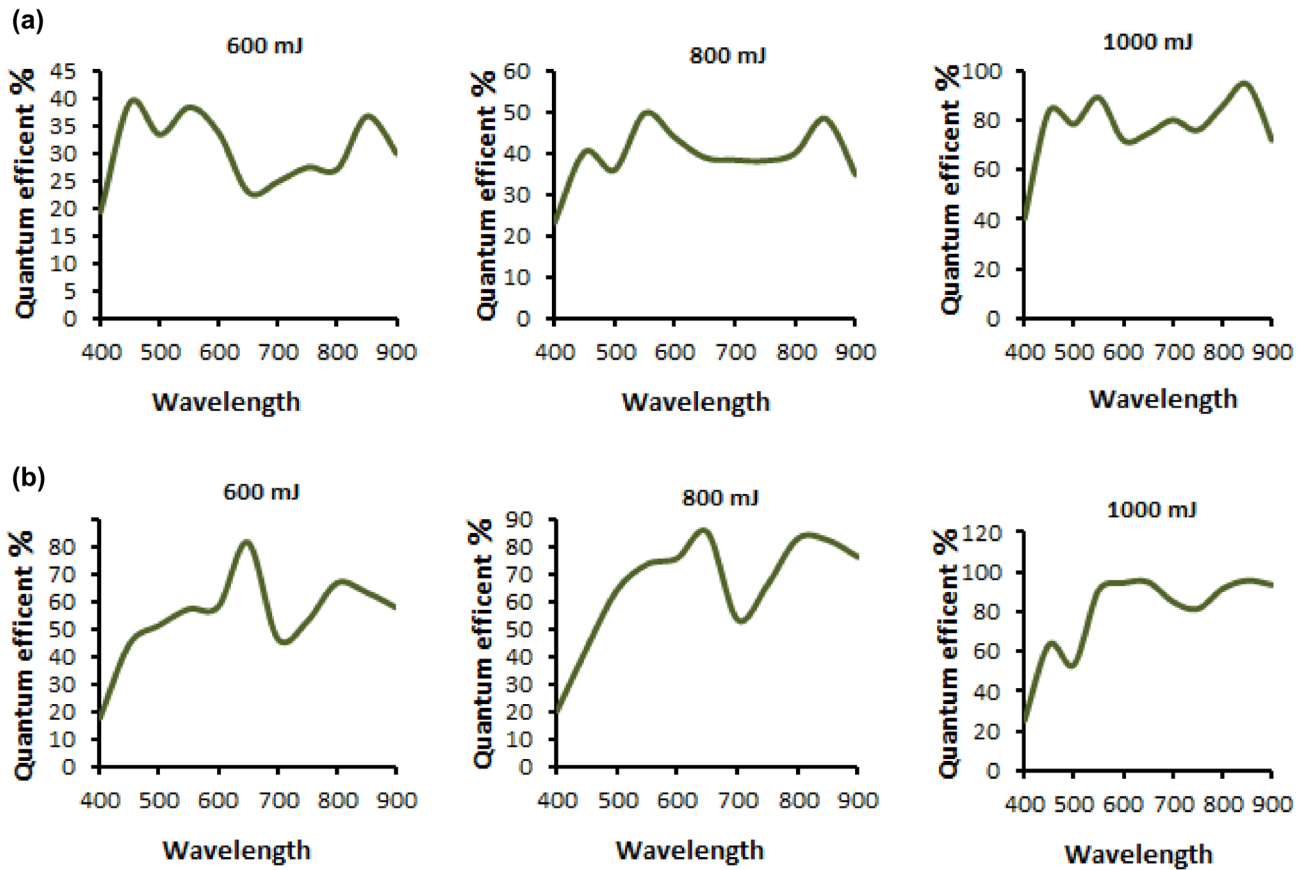
(a)

(b)

Fig. 11 Quantum efficiency of AuNPs produced on PS substrate with varied laser wavelength (**a**) 532 nm, (**b**) 1064 nm

quantum efficiency of relationships inside a system determines it.

Conclusion

The pore size of porous silicon (PS) films increases as the laser wavelength decreases; from the (*J–V*) characteristic, it is evident that the current increased when AuNPs were present. At laser energy of 600, 800, and 1000 mJ ablated on the PS layer. This is caused by the AuNPs high conductivity of the layer, this due to the current rise in comparison the PS sample and decrease in comparison with bulk Si. When employing PS layer instead of c-Si, the responsibility has improved, and it has improved even more after doping the AuNPs. The AuNPs can be deposited on the PS surface to assist improve light absorption, reduce resistance, and improve overall conversion efficiency. These findings show that a low-cost visible photodetector based on this high-quality photodiode could be a feasible option in commercial photoelectric applications.

References

1. N. Hanzic, T. Jurkin, A. Maksmovic, M. Gotic, The synthesis of gold nanoparticles by citrateradiolytical method. J. Radiat. Phys. Chem. **106**, 77–82 (2015)
2. T. Rashid, U. Nayef, M. Jabir, F.A.-H. Mutlak, Study of optical and morphological properties for Au-ZnO nanocomposite

prepared by laser ablation in liquid. J. Phys. Conf. Ser. **1795**, 012041 (2021)

3. M. Abed, F.A.-H. Mutlak, A. Ahmed, U. Nayef, S. Abdulridha, M. Jabir, Synthesis of Ag/Au (core/shell) nanoparticles by laser ablation in liquid and study of their toxicity on blood human components. J. Phys. Conf. Ser. **1795**, 012013 (2021)

4. M. Sainato, L. Strambini, S. Rella, E. Mazzotta, G. Barillaro, Sub-parts per million NO_2 chemi-transistor sensors based on composite porous silicon/gold nanostructures prepared by metal-assisted etching. ACS Appl. Mater. Interfaces **7**, 7136–7145 (2015)

5. A. Ahmed, M. Abdulameer, M. Kadhim, F. Mutlak, Plasma parameters of Au nano-particles ablated on porous silicon produced via Nd-YAG laser at 355 nm for sensing NH_3 gas. Optik **249**, 168260 (2022)

6. L. He, Z. Jia, J. Zhou, H. Zhang, X. Lv, D. Sun, Enhancement of the quantum dot fluorescence intensity by Au nanoparticle decoration of a porous silicon photonic crystal. Appl. Phys. B Lasers Opt **123**, 153 (2017)

7. M.B. de la Mora, J. Bornacelli, R. Nava, R. Zanella, J.A. Reyes-Esqueda, Porous silicon photoluminescence modification by colloidal gold nanoparticles: plasmonic, surface and porosity roles. J. Lumin **146**, 247–255 (2014)

8. A. Sunatkari, S. Talwatkar, Y. Tamgadge, G. Muley, Synthesis, characterization and optical properties of L-Arginine stabilized gold nanocolloids. J. Nanosci. Nanotechnol. **5**(2), 30–35 (2015)

9. M. Murawska, A. Skrzypczak, M. Kozak, Structure and morphology of gold nanoparticles in solution studied by TEM, SAXS and UV-Vis. Acta Physicapolonica **121**(4), 888–892 (2012)

10. M. Daniel, D. Astruc, Gold nanoparticles: assembly, supramoleclar chemistry, quantum-size related properties and application toward biology, catalysis and nanotechnology. Chem. Rev. **104**(1), 293–346 (2004)

11. H. Krishna, C. Favazza, A. Gangopadhyay, R. Kalyanaraman, Functional nanostructures through nanosecond laser dewetting of thin metal films. JOM **60**, 37–42 (2008)

12. N. Harb, F. Mutlak, Production and characterization of porous silicon via laser-assisted etching: effect of gamma irradiation. Optik **246**, 167800 (2021)

13. H.K. Abood, F. Mutlak, Structural, morphological and optical properties of n-type porous silicon-effect of etching current density. IOP Conf. Ser. Mater. Sci. Eng. **757**, 012065 (2020)

14. F. Mutlak, A. Ahmed, U. Nyef, Q. Al-zaidi, S. Abdulridha, Improvement of absorption light of laser texturing on silicon surface for optoelectronic application. Optik **237**, 166755 (2021). https://doi.org/10.1016/j.ijleo.2021.166755

15. Y. Oh, J. Kim, C. Thompson, C. Ross, Templated assembly of Co–Pt nanoparticlesvia thermal and laser-induced dewetting of bilayer metal films. Nanoscale **5**(1), 401–407 (2013)

16. M. Kawasaki, M. Hori, Laser-induced conversion of noble metal-island films to dense monolayers of spherical nanoparticles. J. Phys. Chem. B **107**, 6760–6765 (2003)

17. Y.Y. Wu, J. Fowlkes, P. Rack, J. Diez, L. Kondic, On the breakup of patterned nanoscale copper rings into droplets via pulsed-laser-induced dewetting: competing liquid-phase instability and transport mechanisms. Langmuir **26**, 11972–11979 (2010)

18. J. Fowlkes, L. Kondic, J. Diez, Y. Wu, P.D. Rack, Self-assembly versus directed assembly of nanoparticles via pulsed laser induced dewetting of patterned metal films. Nano Lett. **11**, 2478–2485 (2011)

19. J. Yoo, K. Lee, P. Schmuki, Dewetted Au films form a highly active photocatalytic system on TiO2 nanotube-stumps. Electrochem. Commun. **34**, 351–355 (2013)

20. J.Z. Dong, J. Ye, D. Ariyanti, Y. Wang, S. Wei, W. Gao, Enhancing photocatalytic activities of titanium dioxide via well-dispersed copper nanoparticles. Chemosphere **204**, 193–201 (2018)

21. H. Krishna, N. Shirato, C. Favazza, R. Kalyanaraman, Pulsed laser induced self-organization by dewetting of metallic films. J. Mater. Res **26**(2), 154–169 (2011)

22. M. Garcia, Surface plasmons in metallic nanoparticles: fundamentals and applications. J. Appl. Phys. **44**, 283001–283019 (2011)

23. F.A.-H. Mutlak, R. Jamal, A. Ahmed, Pulsed laser deposition of TiO_2 nanostructures for verify the linear and non-linear optical characteristics. Iraqi J. Sci. **62**(2), 517–525 (2021)

24. B. Chichkov, C. Momma, S. Nolte, F. Von Alvensleben, A. Tünnermann, Femtosecond, picosecond and nanosecond laser ablation of solids. Appl. Phys. A **63**, 109–115 (1996)

25. D. Feldheim, C. Keating, Self assembly of single electron transistors and related devise. Chem. Soc. ReV **27**, 1–12 (1998)

26. D. Gittins, D. Bethell, D. Schiffrin, R. Nichols, A nanometre-scale electronic switch consisting of a metal cluster and redox-addressable groups. Nature **408**, 67–69 (2000)

27. D. Boyer, P. Tamarat, A. Maali, B. Lounis, M. Orrit, Photothermal imaging of nanometer-sized metal particles among scatterers. Science **297**, 1160–1163 (2002)

28. D. Yelin, D. Oron, S. Thiberge, E. Moses, Y. Silberberg, Multiphoton plasmon-resonance microscopy. Opt. Express **11**(12), 1385–1391 (2003)

29. B. Schneider, E. Dickinson, E.M. Vach, J. Hoijer, L. Howard, Optical chip immunoassay for hCG in human whole blood. Biosens. Bioelectron. **2000**(15), 597–604 (2000)

30. J. Nam, C. Thaxton, C. Mirkin, Nanoparticle-based bio-bar codes for the ultrasensitive detection of proteins. Science **301**(5641), 1884–1886 (2003)

31. A. Henglein, Physicochemical properties of small metal particles in solution: "microelectrode" reactions, chemisorption, composite metal particles, and the atom-to-metal transition. J. Phys. Chem. **97**, 5457–5471 (1993)

32. P. Kamat, Photophysical, photochemical and photocatalytic aspects of metal nanoparticles. Phys. Chem. B **106**, 7729–7744 (2002)

33. A. Jackson, J. Myerson, F. Stellacci, Spontaneous assembly of subnanometre-ordered domains in the ligand shell of monolayer-protected nanoparticles. Nat. Mater **3**, 330–336 (2004)

34. P. Sudeep, B. Ipe, K. Thomas, M. George, S. Barazzouk, S. Hotchandani, P. Kamat, Ullerene-functionalized gold nanoparticles: a self-assembled photoactive antenna-metal nanocore assembly. Nano Lett. **2**, 29–35 (2002)

35. M. Danial, D. Astruc, Gold nanoparticles: assembly, supramolecular chemistry, quantum-size-related properties, and applications toward. Chem. Rev. **104**, 293–346 (2004)

36. J. Wilcoxon, J. Martin, F. Parsapour, B. Wiedenman, D.F. Kelley, Photoluminescence from nanosize gold clusters. J. Chem. Phys. **108**, 9137 (1998)

37. D. Handley, in *Colloidal Gold: "Principles, Methods and Applications"*, ed. by M. Hayat (Academic, 1989), pp. 1–12

38. G. Compagnini, M.E. Fragala, L. D'urso, C. Spinella, O. Puglisi, Formation and characterization of high-density silver nanoparticles embedded in silica thin films by "in situ" self-reduction. J. Mater. Res. **16**(10), 2934 (2001)

39. F. Mafune, J. Kohno, Y. Takeda, T. Kondow, Formation of gold nanoparticles by laser ablation in aqueous solution of surfactant. J. Phys. Chem. B **105**, 5114 (2001)

40. F. Mafune, J. Kohno, Y. Takeda, T. Kondow, H. Sawabe, Formation and size control of silver nanoparticles by laser ablation in aqueous solution. J. Phys. Chem. B **104**, 9111 (2000)

41. D. Jwied, U. Nayef, F.A.-H. Mutlak, Preparation and characterization of C: Se nano-rods ablated on porous silicon. Optik **239**, 166811 (2021)

42. N.R. Abdulhameed, H.A. Salih, K.I. Hasson, A.K. Ali, Plasmonic absorption of gold and silver nanoparticles in water. Eng. Technol. J. **32**(6 Part (B)) (2014)

43. M. Soriano, R. Palomero, M. Valcárcel, Ionic-liquid-based micro-extraction method for the determination of silver nanoparticles in consumer products. Anal. Bioanal. Chem. **411**(20), 5023–5031 (2019)

44. D. Saida, A. Alibc, M. Khayyatd, M. Boustimib, M. Louloub, R. Seoudi, Study of the influence of plasmonic resonance of gold nanoparticle doped PEDOT: PSS on the performance of organic solar cells based on CuPc/C60. Heliyon **5**(11), e02675 (2019)

45. X. Huang, X. Hu, S. Song, D. Mao, J. Lee, K. Koh, H. Chen, Tripleenhanced surface plasmon resonance spectroscopy based on cell membrane and folic acid functionalized gold nanoparticles for dual-selective circulating tumor cell sensing. Sens. Actuators B Chem. **305**, 127543 (2020)

46. K. Chan, D. Yang, B. Demir, A. Mouritz, H. Lin, B. Jia, K. Lau, Boosting the electrical and mechanical properties of structural dielectric capacitor composites via gold nanoparticle doping. Compos. Part B Eng. **178**, 107480 (2019)

47. A. Deniz, H. Vural, B. Ortaç, T. Uyar, Gold nanoparticle/polymer nanofibrous composites by laser ablation and electrospinning. Mater. Lett. **65**, 2941–2943 (2011)

48. D. Idisi, H. Ali, J. Oke, S. Sarma, S. Moloi, S. Ray, A. Strydom, Electronic, electrical and magnetic behaviours of reduced graphene-oxide functionalized with silica coated gold nanoparticles. Appl. Surf. Sci. **483**, 106–113 (2019)

49. S. Link, M. Sayed, Optical properties and ultrafast dynamics of metallic nanocrystals. Annu. Rev. Phys. Chem. **54**(1), 331–366 (2013)

50. R. He, X. Qian, J. Yin, Z. Zhu, Preparation of polychrome silver nanoparticles in different solvents. J. Mater. Chem. **12**(12), 3783–3786 (2003)

51. R. Das, S. Nath, D. Chakdar, G. Gope, R. Bhattacharjee, Preparation of silver nanoparticles and their characterization. J. Nanotechnol. **5**, 1–6 (2009)

52. A. Talib, C. Petit, M. Pileni, Optical properties of self-assembled 2D and 3D superlattices of silver nanoparticles. J. Phys. Chem. B **102**(12), 2214–2220 (1998)

53. M. Kim, S. Osone, T. Kim, H. Higashi, T. Seto, "Synthesis of nanoparticles" by laser ablation: a review. KONA Powder Part. J. **10**(34), 80–90 (2016)

54. A. Hahn, S. Barcikowski, B.N. Chichkov, Influences on nanoparticle production during pulsed laser ablation. J. Laser Micro/Nanoeng. **3**(2), 73–77 (2008)

55. A. Singh, J. Vihinen, E. Frankberg, L. Hyvärinen, M. Honkanen, E. Levänen, Pulsed laser ablation-induced green synthesis of TiO_2 nanoparticles and application of novel small angle X-ray scattering technique for nanoparticle size and size distribution analysis. Nanoscale Res. Lett. **11**(1), 1–9. Phys. Chem. B, **102**(12), 2214 (2016).

56. T. Rashid, U. Nayef, M. Jabir, F.A.-H. Mutlak, Synthesis and characterization of Au:ZnO (core:shell) nanoparticles via laser ablation. Optik **244**, 167569 (2021)

57. M. Aswad, F.A.-H. Mutlak, M. Jabir, S. Abdulridha, A. Ahmed, U. Nayef, Laser assisted hydrothermal synthesis of magnetic ferrite nanoparticles for biomedical applications. J. Phys. Conf. Ser. **1795**, 012030 (2021)

58. D. Jwied, U. Nayef, F.A.-H. Mutlak, Synthesis of C: Se nanoparticles ablated on porous silicon for sensing NO2 and NH3 gases. Optik **241**, 167013 (2021)

59. D. Jwied, U. Nayef, F.A.-H. Mutlak, Synthesis of C: Se nanoparticles via laser ablated with magnetic field on porous silicon for gas sensor applications. Optik **242**, 167207 (2021). https://doi.org/10.1016/j.ijleo.2021.167207

60. F.A.-H. Mutlak, Photovoltaic enhancement of Si micro- and nano-structure solar cells via ultrafast laser texturing. Turk. J. Phys. **38**, 130 (2014)

61. S. Khudiar, U. Nayef, F.A.-H. Mutlak, S. Abdulridha, Characterization of NO_2 gas sensing for ZnO nanostructure grown hydrothermally on porous silicon. Optik **249**, 168300 (2022)

62. N. Harb, F. Mutlak, Effect of laser wavelength on the characterization of V_2O_5 NPs/PS photodetector synthesized by pulsed laser deposition. Optik **258**, 168953 (2022)

63. S. Khudiar, F. Mutlak, U. Nayef, Synthesis of ZnO nanostructures by hydrothermal method deposited on porous silicon for photo-conversion application. Optik **247**, 167903 (2021)

64. N. Harab, F. Mutlak, Effect of etching current density on spectroscopic, structural and electrical properties of porous silicon photodetector. Optik **249**, 168298 (2021)

65. S. Khudiar, U. Nayef, F. Mutlak, Improvement of spectral responsivity of ZnO nanoparticles deposited on porous silicon via laser ablation in liquid. Optik **244**, 167530 (2021)

66. A. Alber, F. Mutlak, The role of various etching time in Si nanostructures for ultra-high sensitivity photodetector. Optik **265**, 169427 (2022)

67. A. Ahmed, W. Yaseen, Q. Abbas, F. Mutlak, Plasma treatment effect on SnO2–GO nano-heterojunction: fabrication, characterization and optoelectronic applications. Appl. Phys. A **127**, 746 (2021)

68. D. Jwied, U. Nayef, F. Mutlak, Improvement of responsivity of C: Se nanoparticles ablated on porous silicon. Optik **241**, 167222 (2021)